PAPER • OPEN ACCESS

Two-way interconversion of millimeter-wave and optical fields in Rydberg gases

To cite this article: Martin Kiffner *et al* 2016 *New J. Phys.* **18** 093030

New Journal of Physics
The open access journal at the forefront of physics

Deutsche Physikalische Gesellschaft DPG
IOP Institute of Physics

Published in partnership with: Deutsche Physikalische Gesellschaft and the Institute of Physics

CrossMark

OPEN ACCESS

RECEIVED
26 September 2016

ACCEPTED FOR PUBLICATION
4 October 2016

PUBLISHED
24 October 2016

CORRIGENDUM

Corrigendum: Two-way interconversion of millimeter-wave and optical fields in Rydberg gases (2016 *New J. Phys.* **18** 093030)

Martin Kiffner[1,2], **Amir Feizpour**[2], **Krzysztof T Kaczmarek**[2], **Dieter Jaksch**[1,2] **and Joshua Nunn**[2]

[1] Centre for Quantum Technologies, National University of Singapore, 3 Science Drive 2, 117543, Singapore
[2] Clarendon Laboratory, University of Oxford, Parks Road, Oxford OX1 3PU, UK

E-mail: martin.kiffner@physics.ox.ac.uk

The correct figure 5, with two amended labels, appears below.

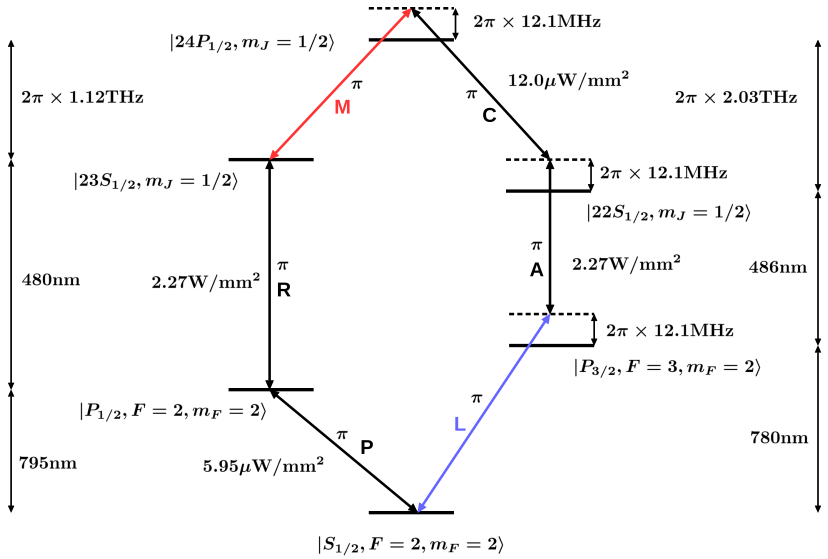

Figure 5. Realisation of the level scheme in figure 1 based on transitions in ^{87}Rb. All quantum numbers of the employed states as well as intensities, polarisations and detunings are indicated. Note that energy spacings are not to scale. The intensities and detunings correspond to the parameters in figure 2. The decay rate $\gamma = 2\pi \times 6.1$ MHz corresponds to the D_2 line. We set the decay rate Γ of all Rydberg states equal to the decay rate of the $|23S_{1/2}\rangle$ state at $T = 300$ K which is faster than the decay rate of the $|24P_{1/2}\rangle$ state. We find [46] $\Gamma/\gamma = 1/285$ and the ratio of the coupling constants is $b = \sqrt{0.72}$.

New Journal of Physics
The open access journal at the forefront of physics

Deutsche Physikalische Gesellschaft DPG
IOP Institute of Physics

Published in partnership with: Deutsche Physikalische Gesellschaft and the Institute of Physics

OPEN ACCESS

RECEIVED
23 May 2016

REVISED
4 August 2016

ACCEPTED FOR PUBLICATION
31 August 2016

PUBLISHED
15 September 2016

PAPER

Two-way interconversion of millimeter-wave and optical fields in Rydberg gases

Martin Kiffner[1,2,3], **Amir Feizpour**[2], **Krzysztof T Kaczmarek**[2], **Dieter Jaksch**[1,2] **and Joshua Nunn**[2]

[1] Centre for Quantum Technologies, National University of Singapore, 3 Science Drive 2, 117543, Singapore
[2] Clarendon Laboratory, University of Oxford, Parks Road, Oxford OX1 3PU, UK
[3] Author to whom any correspondence should be addressed.

E-mail: martin.kiffner@physics.ox.ac.uk

Keywords: frequency conversion, terahertz detection, Rydberg atoms

Supplementary material for this article is available online

Abstract

We show that cold Rydberg gases enable an efficient six-wave mixing process where terahertz or microwave fields are coherently converted into optical fields and vice versa. This process is made possible by the long lifetime of Rydberg states, the strong coupling of millimeter waves to Rydberg transitions and by a quantum interference effect related to electromagnetically induced transparency. Our frequency conversion scheme applies to a broad spectrum of millimeter waves due to the abundance of transitions within the Rydberg manifold, and we discuss two possible implementations based on focussed terahertz beams and millimeter wave fields confined by a waveguide, respectively. We analyse a realistic example for the interconversion of terahertz and optical fields in rubidium atoms and find that the conversion efficiency can in principle exceed 90%.

1. Introduction

Two-way conversion between optical fields and terahertz/microwave radiation is a highly desirable capability with applications in classical and quantum technologies, including the metrological transfer of atomic frequency standards [1], novel astronomical surveys [2], long-distance transmission of electronic data via photonic carriers [3], and signal processing for applications in radar and avionics [4]. Efficient conversion of terahertz radiation into visible light would facilitate the generation, detection and imaging of terahertz fields [5, 6] for stand-off detection, biomedical diagnostics and spectroscopy. In the quantum domain, coherent microwave-optical conversion could enable quantum computing via optically-mediated entanglement swapping [7–9] in solid state systems such as spins in silicon [10] or superconducting qubits [11], which lack optical transitions but couple strongly to microwaves. Moreover, Josephson junctions can mediate microwave photonic nonlinearities that cannot easily be replicated for optical photons [12] so that coherent microwave-optical conversion also provides a route to freely-scalable all-photonic quantum computing.

Recent proposals for conversion between the optical and mm-wave domains have been based on optomechanical transduction [13–15], or frequency mixing in Λ-type atomic ensembles [16–20]. Both approaches require high quality frequency-selective cavities limiting the conversion bandwidth, as well as aggressive cooling or optical pumping to bring the conversion devices into their quantum ground states.

In this paper, we propose instead to use frequency mixing in Rydberg gases [21–23] for the conversion of millimeter waves to optical fields (MMOC) (see figure 1). We use the terminology 'mm-wave' broadly to refer to fields with carrier frequencies between 10 and 10 000 GHz, corresponding to resonant transitions between highly excited Rydberg states in an atomic vapour. Our scheme benefits from the strong coupling between Rydberg atoms and millimeter waves which has previously been used for detection and magnetometry [24–26], storage of microwaves [27] and hybrid atom–photon gates [28]. Here we show how to achieve efficient and coherent MMOC without the need for cavities, microfabrication or cooling. Our MMOC scheme is made possible by an electromagnetically induced transparency (EIT)-related quantum interference effect and the long lifetime of

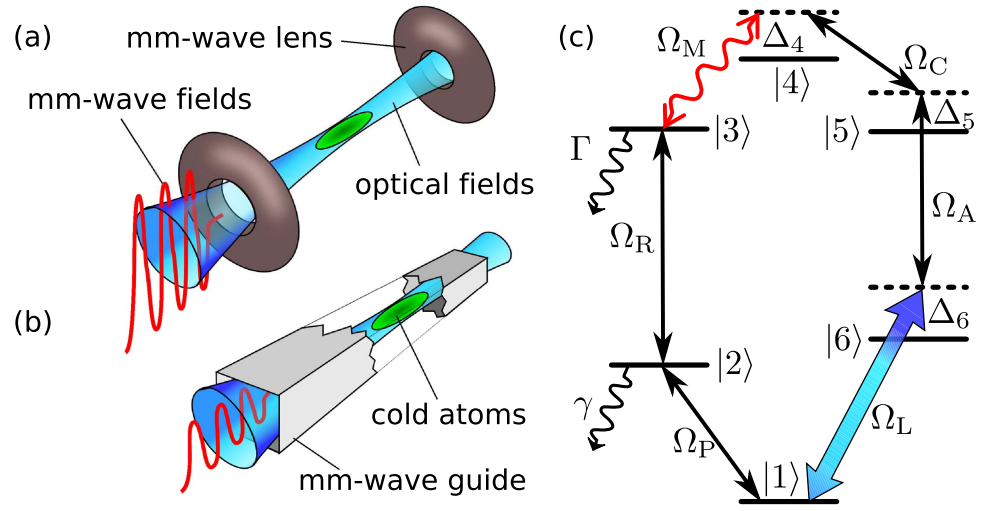

Figure 1. (a) and (b) depict two possible implementations of the considered MMOC device where a mm-wave field (red) and an optical field (blue) are coherently interconverted through their interaction with an ensemble of cold atoms (green). The other fields needed to drive the interaction are not shown. (a) The mm-wave fields are coupled into and out of the atomic ensemble with dielectric lenses; the optical fields are directed through small, sub-mm holes. (b) Tight confinement of microwaves with longer wavelengths could be achieved by trapping the atoms inside the core of a hollow waveguide. (c) Atomic level scheme. Transition frequencies and detunings are not to scale. Ω_M and Ω_L are the Rabi frequencies associated with the mm-wave and the optical fields, respectively. Ω_P, Ω_R, Ω_C and Ω_A are Rabi frequencies of the auxiliary fields, and Δ_k is the detuning of the fields with state $|k\rangle$ ($k \in \{4, 5, 6\}$). Levels $|3\rangle$, $|4\rangle$ and $|5\rangle$ are Rydberg states with decay rate $\Gamma \ll \gamma$, where γ is the decay rate of states $|2\rangle$ and $|6\rangle$.

the Rydberg states. In contrast to previous frequency mixing schemes in EIT media [29–31], this quantum interference effect implements a coherent beam splitter interaction between the millimeter and optical fields which underpins the conversion effect. Our main result is a theoretical model establishing the principle of operation of the proposed device, which it is shown could be implemented in an ensemble of cold trapped Rb atoms.

The paper is organised as follows. We introduce our theoretical model based on the standard framework of coupled Maxwell–Bloch equations in section 2, where we also describe how to include interactions between Rydberg atoms. In section 3 we discuss the principle of operation of our scheme and show that both time-independent and pulsed input fields of arbitrary (band-limited) shape can be efficiently converted. We go on to consider the simultaneous spatial confinement of mm-wave and optical fields, and we show that high conversion efficiencies are predicted for a realistic implementation in trapped Rb vapour. A brief summary of our work is presented in section 4.

2. Model

We consider an ensemble of cold trapped atoms interacting with laser fields and mm-waves and model these interactions using the standard framework of coupled Maxwell–Bloch equations. A summary of the general approach is presented in section 2.1, and a detailed derivation can be found in the supplementary information. The analytical solution of the Maxwell–Bloch equations is outlined in section 2.2 and complemented by appendix. In section 2.3 we include Rydberg–Rydberg interactions into our model. This allows us to identify parameter regimes in section 3 where these interactions are negligible.

2.1. Maxwell–Bloch equations

In a first step we neglect atom–atom interactions and consider the Bloch equations for a single atom with level scheme as shown in figure 1. The millimeter wave Ω_M of interest couples to the transition $|3\rangle \leftrightarrow |4\rangle$, where $|3\rangle$ and $|4\rangle$ are Rydberg states with principal quantum number $n \gtrsim 20$. The optical field Ω_L of interest couples to the $|1\rangle \leftrightarrow |6\rangle$ transition, and the conversion between Ω_M and Ω_L is facilitated by four auxiliary fields. The resonant fields Ω_P and Ω_R create a coherence on the $|1\rangle \leftrightarrow |3\rangle$ transition through coherent population trapping [32]. The two other auxiliary fields Ω_C and Ω_A are in general off-resonant and establish a coherent connection between the $|3\rangle \leftrightarrow |4\rangle$ and $|1\rangle \leftrightarrow |6\rangle$ transitions. We model the time evolution of the atomic density operator by a Markovian master equation

$$\partial_t \varrho = -\frac{\mathrm{i}}{\hbar}[H, \varrho] + \mathcal{L}_\gamma \varrho. \tag{1}$$

In the electric-dipole and rotating-wave approximations, the Hamiltonian H in equation (1) is given by

$$\begin{aligned} H &= -\hbar\sum_{k=3}^{6}\Delta_k A_{kk} - \hbar\left(\Omega_{\rm P}A_{21} + \Omega_{\rm R}A_{32} + \Omega_{\rm M}A_{43}\right. \\ &\quad \left. + \Omega_{\rm C}A_{45} + \Omega_{\rm A}A_{56} + \Omega_{\rm L}A_{61} + \text{h.c.}\right), \end{aligned} \tag{2}$$

and $A_{ij} = |i\rangle\langle j|$ are atomic transition operators. The detuning Δ_k in equation (2) is defined as

$$\Delta_3 = \omega_{\rm P} + \omega_{\rm R} - \omega_3, \tag{3a}$$

$$\Delta_4 = \omega_{\rm P} + \omega_{\rm R} + \omega_{\rm M} - \omega_4, \tag{3b}$$

$$\Delta_5 = \omega_{\rm P} + \omega_{\rm R} + \omega_{\rm M} - \omega_{\rm C} - \omega_5, \tag{3c}$$

$$\Delta_6 = \omega_{\rm L} - \omega_6, \tag{3d}$$

where $\hbar\omega_k$ denotes the energy of state $|k\rangle$ with respect to the energy of level $|1\rangle$ and ω_X is the frequency of field X with Rabi frequency Ω_X ($X \in \{\text{P, R, C, A, M, L}\}$). The term $\mathcal{L}_\gamma\varrho$ in equation (1) accounts for spontaneous emission from the excited states. These processes are described by standard Lindblad decay terms. The full decay rate of the states $|2\rangle$ and $|6\rangle$ is γ, and the long-lived Rydberg states decay with $\Gamma \ll \gamma$. The six fields drive a resonant loop

$$\omega_{\rm P} + \omega_{\rm R} + \omega_{\rm M} - \omega_{\rm C} - \omega_{\rm A} - \omega_{\rm L} = 0, \tag{4}$$

and we impose the phase matching condition

$$\boldsymbol{k}_{\rm P} + \boldsymbol{k}_{\rm R} + \boldsymbol{k}_{\rm M} - \boldsymbol{k}_{\rm C} - \boldsymbol{k}_{\rm A} = \boldsymbol{k}_{\rm L}. \tag{5}$$

In the following, we assume that $\Omega_{\rm M}$ and $\Omega_{\rm L}$ are co-propagating, while the directions of the auxiliary fields are chosen such that equation (5) holds. Note that this phase matching condition is automatically fulfilled by virtue of equation (4) if all fields are co-propagating.

The strong auxiliary fields are not significantly affected by their interaction with the mm-wave and optical signals. We therefore consider only these signal fields and the atomic coherences as dynamical variables. In the paraxial approximation we find

$$\left(-\frac{\rm i}{2k_{\rm M}}\Delta_\perp + \frac{1}{c}\partial_t + \partial_z\right)\Omega_{\rm M} = {\rm i}\eta_{\rm M}\varrho_{43}, \tag{6a}$$

$$\left(-\frac{\rm i}{2k_{\rm L}}\Delta_\perp + \frac{1}{c}\partial_t + \partial_z\right)\Omega_{\rm L} = {\rm i}\eta_{\rm L}\varrho_{61}, \tag{6b}$$

where $k_{\rm M}$ ($k_{\rm L}$) is the wavenumber of the mm-wave (optical) field and $\Delta_\perp = \partial_x^2 + \partial_y^2$ is the transverse Laplace operator. The coupling constants $\eta_{\rm M}$ and $\eta_{\rm L}$ are given by

$$\eta_{\rm M} = \mathcal{N}\frac{|\boldsymbol{d}_{43}|^2}{2\hbar\epsilon_0 c}\omega_{\rm M}, \tag{7a}$$

$$\eta_{\rm L} = \mathcal{N}\frac{|\boldsymbol{d}_{61}|^2}{2\hbar\epsilon_0 c}\omega_{\rm L}, \tag{7b}$$

where $\boldsymbol{d}_{kl} = \langle k|\hat{\boldsymbol{d}}|l\rangle$ is the matrix element of the electric dipole moment operator $\hat{\boldsymbol{d}}$ on the transition transition $|k\rangle \leftrightarrow |l\rangle$, c is the speed of light and $\mathcal{N}$ is the density of atoms. In the following the ratio of the coupling constants is denoted by

$$b^2 = \eta_{\rm M}/\eta_{\rm L} = \frac{|\boldsymbol{d}_{43}|^2}{|\boldsymbol{d}_{61}|^2}\frac{\omega_{\rm M}}{\omega_{\rm L}}. \tag{8}$$

Numerical solutions of equations (1) and (6) are presented in section 3.3, but first it is instructive to derive analytic solutions in the limit that diffraction over the length of the atomic ensemble can be neglected.

2.2. Analytical solution

The first-order solution of equation (1) with respect to the Rabi frequencies $\Omega_{\rm M}$, $\Omega_{\rm L}$ takes the form (see appendix)

$$\varrho_{43} \approx \chi_{43}^{\rm M}\Omega_{\rm M} + \chi_{43}^{\rm L}\Omega_{\rm L}, \tag{9a}$$

$$\varrho_{61} \approx \chi_{61}^{\rm M}\Omega_{\rm M} + \chi_{61}^{\rm L}\Omega_{\rm L}. \tag{9b}$$

The response of the atomic system on the $|3\rangle \leftrightarrow |4\rangle$ transition induced by the mm-wave field is described by $\chi_{43}^{\rm M}$, and $\chi_{61}^{\rm L}$ accounts for the atomic response on the transition $|1\rangle \leftrightarrow |6\rangle$ due to the optical field. In addition, the mm-wave field can induce a coherence proportional to $\chi_{61}^{\rm M}$ on the optical transition $|1\rangle \leftrightarrow |6\rangle$, and the

optical field can create a coherence proportional to χ_{43}^{L} on the transition $|3\rangle \leftrightarrow |4\rangle$. The cross-terms proportional to χ_{43}^{L} and χ_{61}^{M} in equation (9) originate from the closed-loop character of the atomic level scheme.

Next we combine equation (9) with (6) and make the simplifying assumption that diffraction over the ensemble length can be neglected, so that the transverse Laplacians can be dropped. Making a coordinate transformation from the laboratory frame (t, z) to a frame $(\tau = t - z/c,\ z)$ co-moving with the signal fields, the evolution equation for the mm-wave and optical fields can then be written as

$$\partial_z \boldsymbol{\Omega} = \mathrm{i}\mathcal{M}\boldsymbol{\Omega}, \tag{1}$$

where

$$\mathcal{M} = \eta_{\mathrm{L}} \begin{pmatrix} b^2\chi_{43}^{\mathrm{M}} & b^2\chi_{43}^{\mathrm{L}} \\ \chi_{61}^{\mathrm{M}} & \chi_{61}^{\mathrm{L}} \end{pmatrix}, \quad \boldsymbol{\Omega} = \begin{pmatrix} \Omega_{\mathrm{M}} \\ \Omega_{\mathrm{L}} \end{pmatrix}. \tag{11}$$

When the auxiliary fields are time-independent and spatially uniform, the solution to equation (10) is

$$\boldsymbol{\Omega} = \exp(\mathrm{i}\mathcal{M}z)\boldsymbol{\Omega}_0, \tag{12}$$

where $\boldsymbol{\Omega}_0$ is the initial condition $\boldsymbol{\Omega}$ evaluated at $z = 0$. The matrix exponential in equation (12) can be expressed in terms of the 2×2 identity matrix $\mathbb{1}$ and the Pauli matrices σ_k [33]

$$\exp(\mathrm{i}\mathcal{M}z) = \exp(\mathrm{i}a_0 z)\left[\cos(\sqrt{\boldsymbol{a}^2}z)\mathbb{1} + \mathrm{i}\frac{\boldsymbol{a}\cdot\boldsymbol{\sigma}}{\sqrt{\boldsymbol{a}^2}}\sin(\sqrt{\boldsymbol{a}^2}z)\right], \tag{13}$$

where

$$a_0 = \frac{1}{2}\mathrm{Tr}(\mathcal{M}), \quad \boldsymbol{a} = \frac{1}{2}\mathrm{Tr}(\mathcal{M}\boldsymbol{\sigma}). \tag{14}$$

The solution presented here treats the signal fields Ω_{M}, Ω_{L} as c-numbers. However, the generalisation to quantum fields is straightforward since the coherences in equation (9) are linear in the signal fields. Apart from quantum noise operators, our calculations are thus equivalent to a Heisenberg–Langevin approach where the signal Rabi frequencies Ω_{M}, Ω_{L} are replaced by quantum fields [34–36]. Since the Langevin noise operators represent only vacuum noise, they do not contribute to normally ordered expectation values, which determine the conversion efficiency.

2.3. Interaction-induced imperfections

Next we consider the effects of dipole-mediated interactions between atoms excited into their Rydberg manifolds. In general, Rydberg interactions will prevent some fraction of atoms from participating in the conversion process and lead to absorption of the signal fields, and therefore will reduce the conversion efficiency. The atomic level scheme in figure 1(b) contains three Rydberg states, and the population in state $|3\rangle$ is continuously kept at $\rho_{33} \approx |\Omega_{\mathrm{P}}/\Omega_{\mathrm{R}}|^2$ via coherent population trapping. On the other hand, the population in the other Rydberg states $|4\rangle$ and $|5\rangle$ is negligibly small for weak fields Ω_{M} and Ω_{L}. The dominant perturbation to the conversion mechanism will thus stem from nearby Rydberg atoms in state $|3\rangle$. In order to model this, we consider a system of two atoms where atom A is located at the coordinate origin. The conversion process in atom A is disturbed by Rydberg–Rydberg interactions with atom B, which is prepared in state $|3\rangle$ and positioned at $\boldsymbol{R}$. Next we discuss the two dominant effects caused by the presence of atom B. First, atom B gives rise to a van der Waals shift of state $|3\rangle$ in atom A [37]

$$\hbar\Delta_{\mathrm{vdW}} = -\frac{C_6}{R^6}, \tag{15}$$

where the coefficient C_6 depends on the quantum numbers of state $|3\rangle$. If R is smaller than the blockade radius R_{b}, atom A cannot be excited to the Rydberg state and thus does not participate in the conversion. The blockade radius is determined by the single-atom EIT linewidth $\gamma_{\mathrm{EIT}} = |\Omega_{\mathrm{R}}|^2/\gamma$ and given by $R_{\mathrm{b}} = [2|C_6|/(\hbar\gamma_{\mathrm{EIT}})]^{1/6}$ [38]. Second, atom B gives rise to a frequency shift of state $|4\rangle$ in atom A via the resonant dipole–dipole interaction [39]

$$\hbar\Delta_{\mathrm{DD}} = \frac{1}{4\pi\varepsilon_0}\frac{|\boldsymbol{d}_{43}|^2 - 3|\boldsymbol{d}_{43}\cdot\vec{\boldsymbol{R}}|^2}{R^3}, \tag{16}$$

where $\vec{\boldsymbol{R}} = \boldsymbol{R}/R$. In contrast to the van der Waals shift in equation (15), Δ_{DD} depends on the relative orientation of the two atoms. In principle, state $|5\rangle$ in atom A can experience a similar shift Δ_{DD} if the dipole moment $\boldsymbol{d}_{53}$ is different from zero. Here we assume that states $|5\rangle$ and $|3\rangle$ have the same parity so that $\boldsymbol{d}_{53} = 0$, consistent with the example implementation in Rb that we introduce below in section 3.2.

The preceding discussion shows that Rydberg–Rydberg interactions change the energies of states $|3\rangle$ and $|4\rangle$. In order to incorporate these frequency shifts into our model, we find the general first-order solution of the

atomic coherences in equation (9) for arbitrary detunings and Rabi frequencies of the auxiliary fields. We then introduce the effective detuning parameters

$$\widetilde{\Delta}_3 = \Delta_3 - \Delta_{\rm vdW}, \tag{17a}$$

$$\widetilde{\Delta}_4 = \Delta_4 - \Delta_{\rm DD}, \tag{17b}$$

and replace Δ_3 and Δ_4 in the general expression for the matrix $\mathcal{M}$ in equation (11) by $\widetilde{\Delta}_3$ and $\widetilde{\Delta}_4$. Since $\Delta_{\rm vdW}$ and $\Delta_{\rm DD}$ depend on the relative position $\boldsymbol{R}$, we average $\mathcal{M}$ over $\boldsymbol{R}$

$$\mathcal{M} \longrightarrow \widetilde{\mathcal{M}} = \int \mathrm{d}^3\boldsymbol{R}\ \mathcal{M}(\boldsymbol{R}) w(\boldsymbol{R}), \tag{18}$$

where the distribution of nearest neighbours in a random sample of Rydberg atoms follows the probability density [40]

$$w(\boldsymbol{R}) = \frac{1}{4\pi}\frac{3}{r_{\rm ws}}\left(\frac{R}{r_{\rm ws}}\right)^2 \exp\left[-\left(\frac{R}{r_{\rm ws}}\right)^3\right], \tag{19}$$

with the parameter

$$r_{\rm ws} = \left[\frac{3}{4\pi\mathcal{N}_{\rm Ry}}\right]^{1/3} \tag{20}$$

the Wigner–Seitz radius for a given density of Rydberg atoms $\mathcal{N}_{\rm Ry}$.

This account of Rydberg–Rydberg interactions is expected to work well for weak optical and mm-wave fields. If the intensities of $\Omega_{\rm M}$ and $\Omega_{\rm L}$ are increased such that the population in $|4\rangle$ and $|5\rangle$ is not negligible, other dipole–dipole interactions can occur that are not captured by our model. Furthermore, our model neglects cooperative effects like superradiance [41] and frequency shifts due to a ground state atom within the electron orbit of a Rydberg state [42]. However, experimental results [43–45] for EIT involving a Rydberg state show that these effects can be negligible for low principal quantum numbers $n \lesssim 40$, for weak probe fields and low atomic densities.

3. Results

In a first step we analyse the simplified analytical model of section 2.2 in order to explain the principle of the conversion mechanism. This is presented in section 3.1 where we also investigate the maximally achievable conversion efficiencies. We then introduce one possible implementation of our scheme in rubidium vapour in section 3.2 and find a set of parameters for which Rydberg–Rydberg interactions are negligibly small. Finally, we present numerical results for MMOC in the physical systems shown in figures 1 (a) and (b) in section 3.3.

3.1. Conversion mechanism

The conversion efficiency between mm-wave and optical fields according to equation (12) will be small for a generic matrix $\mathcal{M}$, but complete conversion can be achieved if the atomic ensemble realises a beam splitter interaction

$$V_{\rm BS} \propto (\hat{\Omega}_{\rm M}\hat{\Omega}_{\rm L}^{\dagger} + \hat{\Omega}_{\rm M}^{\dagger}\hat{\Omega}_{\rm L}), \tag{21}$$

where the 'hat' notation emphasises the operator nature of the fields. Formally, such an interaction corresponds to the case where the diagonal elements of $\mathcal{M}$ vanish. We find that this condition, such that $\chi_{43}^{\rm M} \approx \chi_{61}^{\rm L} \approx 0$, can indeed be met if the intensities and detunings of the auxiliary fields satisfy

$$|\Omega_{\rm R}| \gg |\Omega_{\rm P}|, \quad \Delta_5 = \frac{|\Omega_{\rm C}|^2}{\Delta_4}, \quad \Delta_6 = \frac{|\Omega_{\rm A}|^2}{\Delta_5}. \tag{22}$$

To first order in Γ/γ the susceptibilities in equation (9) are then given by

$$\chi_{43}^{\rm M} \approx \mathrm{i}\frac{8}{b^2\gamma}\varepsilon^2, \quad \chi_{43}^{\rm L} \approx \alpha, \tag{23a}$$

$$\chi_{61}^{\rm M} \approx \alpha^*, \quad \chi_{61}^{\rm L} \approx \mathrm{i}\frac{8}{\gamma}\varepsilon_\Gamma, \tag{23b}$$

where

$$\alpha = \frac{\Omega_{\rm C}\Omega_{\rm P}}{\Delta_4\Omega_{\rm A}^*\Omega_{\rm R}}, \tag{24a}$$

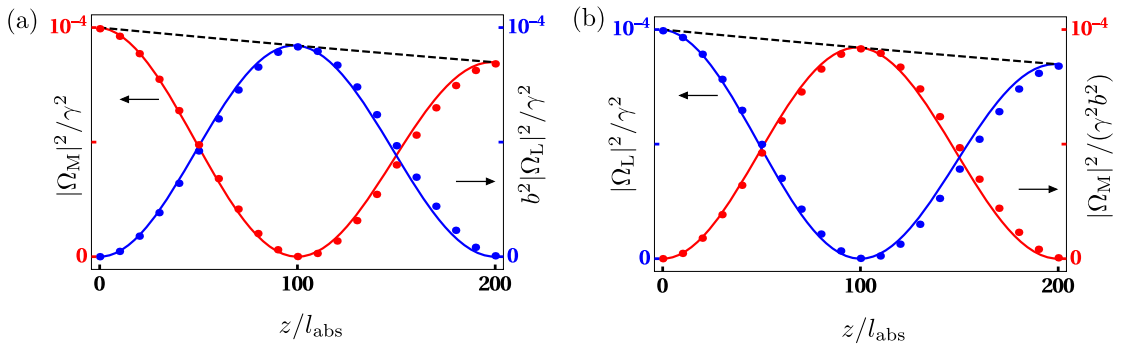

Figure 2. Frequency conversion of stationary fields. Intensities of the millimeter wave (red) and optical field (blue) inside the medium. Dots indicate the results from a numerical integration of Maxwell–Bloch equations. (a) A CW millimeter wave enters the medium at $z = 0$. (b) A CW optical field enters the medium at $z = 0$. In (a) and (b), the dashed line is proportional to the envelope $e^{-2\kappa z}$ and we set $\Gamma/\gamma = 1/285$, $\Omega_A = 2\gamma$, $\Omega_C = 2\gamma$, $\Omega_R = 2\gamma$, $\Omega_P = 0.3\gamma$, $\Delta_4 = 2\gamma$, $\Delta_5 = 2\gamma$, $\Delta_6 = 2\gamma$ and $b = \sqrt{0.72}$. These parameters correspond to the realisation of the level scheme with Rubidium atoms in section 3.2.

$$\varepsilon = \frac{b}{4}\frac{\gamma}{|\Delta_4|}\frac{|\Omega_C|}{|\Omega_A|}\frac{|\Omega_P|}{|\Omega_R|}, \tag{24b}$$

$$\varepsilon_\Gamma = \frac{\Gamma\gamma}{16|\Omega_A|^2}\left(1 + 2\frac{|\Omega_C|^2}{\Delta_4^2}\right). \tag{24c}$$

ε and ε_Γ are dimensionless parameters that are generally smaller than unity. Since $\varepsilon_\Gamma \propto \Gamma$, ε_Γ is typically of the order of ε^2. On the other hand, $|\alpha| \propto \varepsilon$ and hence the off-diagonal elements of the matrix $\mathcal{M}$ are indeed much larger than the diagonal elements.

This result can be understood as follows. The level scheme in figure 1 can be regarded as three consecutive EIT systems where the weak probe fields are represented by Ω_P, Ω_M and Ω_L, respectively. However, these three systems are coupled and hence the normal two-photon resonance condition for transparency of the Ω_M and Ω_L fields is changed. The conditions in equation (22) approximately restore transparency for the field Ω_M (Ω_L) on the transition $|3\rangle \leftrightarrow |4\rangle$ ($|1\rangle \leftrightarrow |6\rangle$) and in the presence of the other levels and fields such that $\chi_{43}^M \approx 0$ ($\chi_{61}^L \approx 0$). However, Ω_M still creates a coherence on the optical transition and Ω_L induces a coherence on the Rydberg transition such that the fields are interconverted as they propagate along the medium. With equations (23) and (24) the general solution for the spatial distribution of the fields in equation (12) is given by

$$\mathbf{\Omega}(z) \approx e^{-\kappa z}\begin{pmatrix} \cos(kz) & ib\sin(kz) \\ \frac{i}{b}\sin(kz) & \cos(kz) \end{pmatrix}\mathbf{\Omega}(0), \tag{25}$$

where $\kappa = (\varepsilon^2 + \varepsilon_\Gamma)/l_{abs}$ and $k = \varepsilon/l_{abs}$ determine the loss and the spatial oscillation period of the interconversion, respectively, $l_{abs} = \gamma/(4\eta_L)$ is the resonant absorption length on the $|6\rangle \leftrightarrow |1\rangle$ transition and we assumed $\varepsilon \ll 1$ and $\varepsilon_\Gamma/\varepsilon \ll 1$.

The spatial oscillations of optical and mm-wave intensities according to equation (25) are shown in figure 2. Our model is in excellent agreement with a full numerical solution of the Maxwell–Bloch equations. Note that the small deviations for large z vanish if the approximations leading to equation (25) are omitted. Complete MMOC occurs after a length $L_c = \pi/(2k)$, and thus requires an optical depth $D_c = L_c/l_{abs}$ that is inversely proportional to ε in equation (24b), $D_c = \pi/(2\varepsilon)$. Since the value of ε can be adjusted through the intensities and frequencies of the auxiliary fields, the condition for complete MMOC can be met for various densities and sizes of atomic gases. In the example in figure 2, we find $L_c = 100 l_{abs}$. The efficiency $F = e^{-2\kappa L_c}$ for complete conversion can be expressed in terms of the optical depth D_c

$$F(D_c) = \exp\left[-\frac{\pi^2}{2D_c}\right]\exp\left[-2\varepsilon_\Gamma D_c\right], \tag{26}$$

and $F(D_c)$ is shown in figure 3 for three different values of ε_Γ. The maximum efficiency $F_{max} = \exp(-2\pi\sqrt{\varepsilon_\Gamma})$ is attained at an optical depth $D_c^{max} = \pi/(2\sqrt{\varepsilon_\Gamma})$ and tends to unity for $\varepsilon_\Gamma \to 0$. Since $\varepsilon_\Gamma \propto \Gamma$, efficiencies close to unity are only possible because of the slow radiative decay rate Γ of the Rydberg levels $|3\rangle$, $|4\rangle$ and $|5\rangle$. Γ decreases with increasing n as $\Gamma \propto n^{-3}$ [46] and is thus typically several orders of magnitude smaller than the decay rate γ of the low-lying states $|2\rangle$ and $|6\rangle$. The efficiency for complete MMOC for the parameters in figure 2 is $F \approx 92.1\%$.

Note that our definition of the efficiency is based on photon fluxes and not intensities as required for a coherent conversion scheme that conserves the total photon flux. In order to see this, we consider the perfectly

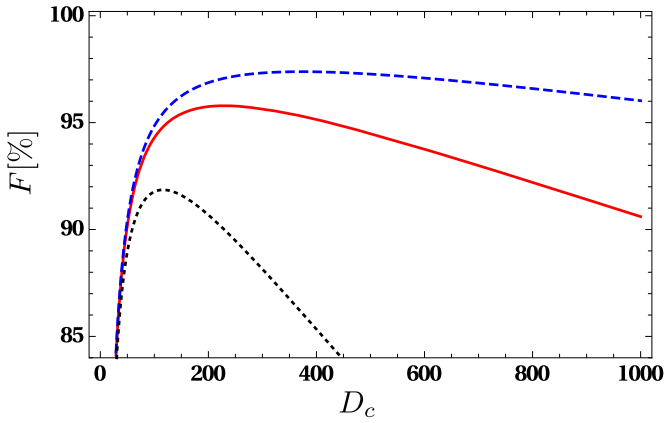

Figure 3. Conversion efficiency as a function of optical depth D_c. We set $\Gamma/\gamma = 3.9 \times 10^{-3}$ (black dotted line), $\Gamma/\gamma = 10^{-3}$ (red solid line) and $\Gamma/\gamma = 3.8 \times 10^{-4}$ (blue dashed line). These parameters correspond to rubidium Rydberg states at zero temperature with $n \approx 20$, $n \approx 30$ and $n \approx 40$, respectively. Common parameters in all three curves are $\Omega_A = 2\gamma$, $\Omega_C = 2\gamma$ and $\Delta_4 = 2\gamma$.

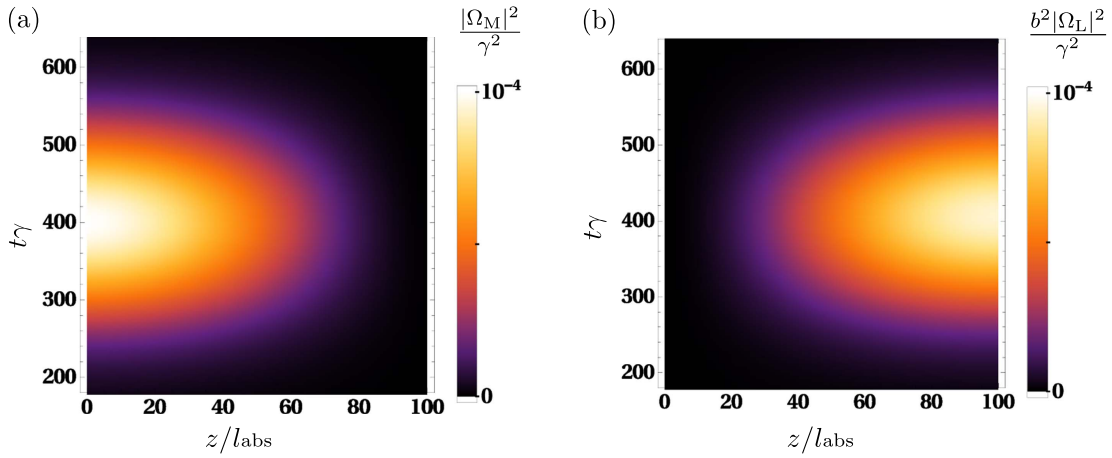

Figure 4. Frequency conversion of pulsed fields. (a) Density plot of the incoming millimeter wave pulse with a Gaussian envelope. (b) Density plot of the outgoing optical pulse. The parameters in (a) and (b) are the same as in figure 2.

coherent conversion of an optical field to a millimeter wave with $F(D_c) = 1$. According to equation (25), we obtain $|\Omega_M(L_c)|^2 = b^2|\Omega_L(0)|^2$. With the definition of b in equation (8) and the definition of the Rabi frequencies we get

$$|\mathcal{E}_M(L_c)|^2 = \frac{\omega_M}{\omega_L}|\mathcal{E}_L(0)|^2, \tag{27}$$

where $\mathcal{E}_M$ and $\mathcal{E}_M$ are the electric field amplitudes of the mm-wave and optical fields, respectively. The ratio of the intensities ($I \propto |\mathcal{E}|^2$) is thus $I_M^{out}/I_L^{in} = \omega_M/\omega_L$, as it should be. Similarly, we obtain $I_L^{out}/I_M^{in} = \omega_L/\omega_M$ for the conversion of mm-waves into optical fields.

Next we consider the conversion of pulsed fields. The derivation of equation (25) shows that our scheme is not mode-selective and works for broadband pulses. The only requirement is that the atomic dynamics remains in the adiabatic regime, which holds if the bandwidth $\delta\nu$ of the input pulse is smaller than all detunings Δ_k and the Rabi frequencies Ω_R, Ω_C and Ω_A (see appendix). In order to demonstrate this, we present numerical solutions of the Maxwell–Bloch equations for a mm-wave input pulse as shown in figure 4. The intensity of a mm-wave input pulse with Gaussian envelope is shown in figure 4(a), and the corresponding optical output field is shown in figure 4(b). The input pulse has a bandwidth on the order of $\Delta\nu \approx 2\pi \times 80$ kHz and is converted without distortion of its shape. We thus find that the bandwidth of our conversion scheme is at least ~80 kHz for the chosen parameters. This bandwidth can be significantly increased by increasing the detunings and Rabi frequencies of the auxiliary fields. Finally, we note that the conversion of optical pulses to mm-waves works equally well.

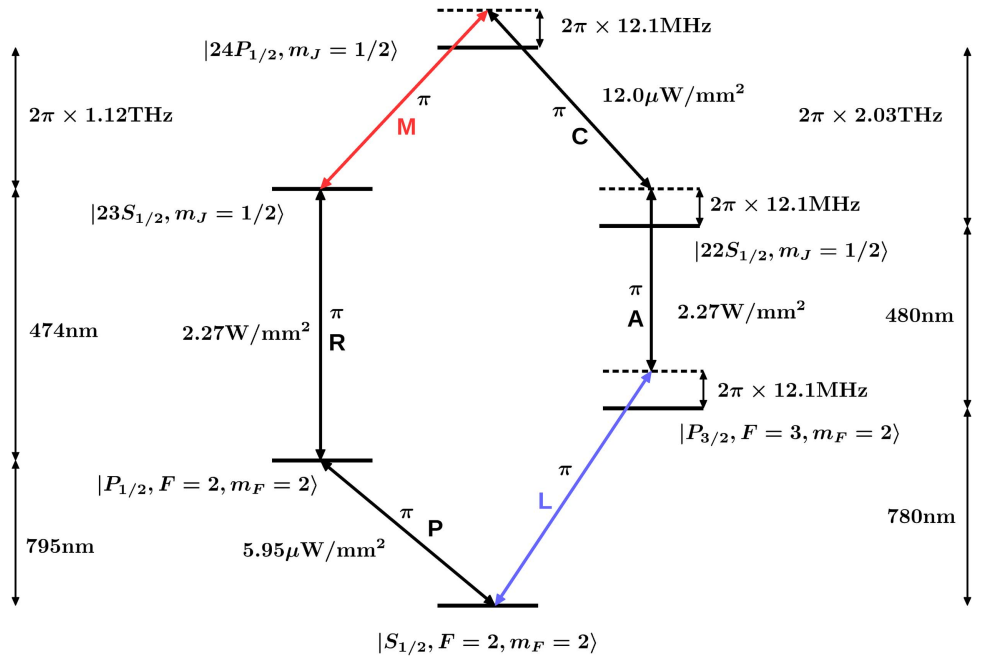

Figure 5. Realisation of the level scheme in figure 1 based on transitions in ^{87}Rb. All quantum numbers of the employed states as well as intensities, polarisations and detunings are indicated. Note that energy spacings are not to scale. The intensities and detunings correspond to the parameters in figure 2. The decay rate $\gamma = 2\pi \times 6.1$ MHz corresponds to the D_2 line. We set the decay rate Γ of all Rydberg states equal to the decay rate of the $|23S_{1/2}\rangle$ state at $T = 300$ K, which is faster than the decay rate of the $|24P_{1/2}\rangle$ state. We find [46] $\Gamma/\gamma = 1/285$ and the ratio of the coupling constants is $b = \sqrt{0.72}$.

3.2. Rubidium parameters

Here we discuss one possible realisation of our scheme based on an ensemble of ^{87}Rb atoms. The atomic level scheme is shown in figure 5, where the optical field L couples to the D_2 line, and the auxiliary P field couples to the D_1 line. The transition dipole matrix elements for the optical transitions can be found in [47], and for transitions between Rydberg states we follow the approach described in [48]. The intensities of the auxiliary fields are chosen such that they correspond to the Rabi frequencies in figure 2, and the values of the detuning parameters in figures 5 and 2 are also equivalent.

Next we show that Rydberg–Rydberg interactions are negligible for the level scheme in figure 5 and for an atomic density of $\mathcal{N} = 2 \times 10^{17}\text{m}^{-3}$. First we note that the Rydberg blockade radius is $R_\text{b} \approx 0.63\ \mu$m for the parameters of figure 5. This is significantly smaller than the mean distance between atoms, and hence the density of Rydberg atoms is simply given by $\mathcal{N}_\text{Ry} \approx \rho_{33}\mathcal{N}$ [49, 50]. By carrying out the average in equation (18), we find that the matrix $\widetilde{\mathcal{M}}$ leads to the same conversion efficiency as $\mathcal{M}$, i.e., there is no notable difference between the curves in figure 2 generated by $\mathcal{M}$ and the corresponding curves produced with $\widetilde{\mathcal{M}}$. On the other hand, if we choose $|3\rangle = |24S_{1/2}, m_J = 1/2\rangle$ instead of $|3\rangle = |23S_{1/2}, m_J = 1/2\rangle$, the conversion efficiency drops to 61%.

In order to obtain more insight into these results, we consider the distance R_{90} where 90% of all Rydberg atom pairs will have a larger separation than R_{90}

$$\int_{R>R_{90}} \text{d}^3\boldsymbol{R}\ w(\boldsymbol{R}) = 0.9. \tag{28}$$

Our parameters give $\mathcal{N}_\text{Ry} \approx 4.4 \times 10^{15}\text{m}^{-3}$ and thus $R_{90} \approx 1.79\ \mu$m. The van der Waals shift between two atoms in state $|3\rangle$ and separated by R_{90} is [37]

$$\Delta_\text{vdW} = -\frac{C_6}{R_{90}^6} \approx 2\pi \times 24.5\ \text{kHz}. \tag{29}$$

This is much smaller than all detuning parameters and Rabi frequencies entering the matrix $\mathcal{M}$. Since the frequency shifts for 90% of all atoms are even smaller, averaging over all nearest neighbour distances does not change the matrix $\mathcal{M}$. Similarly, the dipole–dipole shifts in equation (16) with $|3\rangle = |24S_{1/2}, m_J = 1/2\rangle$ are on the order of

$$\Delta_\text{DD} \propto \frac{1}{4\pi\varepsilon_0\hbar}\frac{|\langle 3|\hat{\boldsymbol{d}}|4\rangle|^2}{R_{90}^3} \approx 2\pi \times 62.6\ \text{kHz}, \tag{30}$$

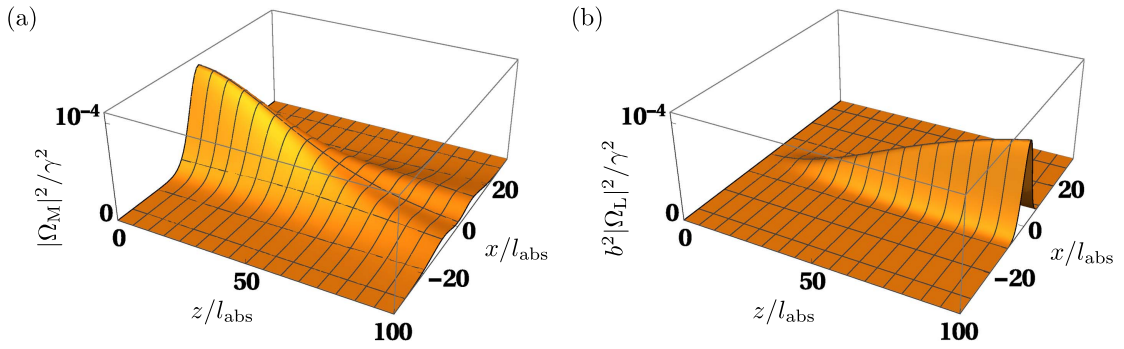

Figure 6. (a) Spatial intensity profile $|\Omega_M|^2$ of an incident mm-wave field in the x–z plane. The beam profile of the mm-wave at $z = 0$ is given by equation (31). (b) Spatial intensity profile $|\Omega_L|^2$ of the resulting generated optical field in the x–z plane. The fields in (a) and (b) are cylindrically symmetric, and the parameters are $\sigma_c = 8l_{abs} \approx 413\ \mu$m, $\sigma_M = 1.9\lambda_M \approx 509\ \mu$m, $\mathcal{N}^{(0)} = 2 \times 10^{17}$ m^{-3} and $\Omega_M^{(0)} = 10^{-4}\gamma$. All other parameters are specified in section 3.2.

which is also small compared to the detuning parameters and Rabi frequencies of the auxiliary fields. On the other hand, Δ_{DD} increases by a factor of 100 by choosing $|3\rangle = |24S_{1/2},\ m_J = 1/2\rangle$ instead of $|3\rangle = |23S_{1/2},\ m_J = 1/2\rangle$. This explains why the conversion efficiency drops significantly by using the strong $|ns\rangle \leftrightarrow |np\rangle$ transition instead of $|(n-1)s\rangle \leftrightarrow |np\rangle$ as in figure 5.

The absorption length for the field L is $l_{abs} = 5.1 \times 10^{-2}$ mm for our parameters. Since full conversion requires an optical depth of ~100, the length of the medium needs to be $L_c \approx 5.1$mm. These parameters are experimentally achievable. For example, much higher optical depths ~1000 have been reported [51, 52], and the atomic cloud size considered here is similar to the dimensions of the experiment in [52], where cold Rb atoms were trapped in a cylindrical geometry of length 4.6 mm and width 0.45 mm.

3.3. Physical implementation

We first consider the setup in figure 1(a) where the mm-wave field is focussed into the atomic ensemble by lenses. We assume that the focal spot is at $z = 0$ such that the mm-wave beam profile is

$$\Omega_M(z = 0,\ r) = \Omega_M^{(0)} e^{-r^2/\sigma_M^2}, \tag{31}$$

where $r = \sqrt{x^2 + y^2}$ is the radial coordinate in the x–y plane, σ_M is the beam waist and $\Omega_M^{(0)}$ is the peak Rabi frequency at the center of the beam. We model the transverse density profile of the atom cloud by a Gaussian with peak density $\mathcal{N}^{(0)}$ and width σ_c

$$\mathcal{N}(r) = \mathcal{N}^{(0)} e^{-2r^2/\sigma_c^2}. \tag{32}$$

In order to calculate the conversion efficiency, we find the stationary solution of equation (6) with the boundary condition in equation (31), the density profile in equation (32) and with the analytical expression for the atomic coherences in equation (23). The result for the parameters specified in section 3.2 is shown in figure 6, where we consider a beam waist of $\sigma_M = 1.9\lambda_M$ and an atomic cloud with transverse size $\sigma_c \approx 413\ \mu$m. The intensity of the millimeter wave is shown in figure 6(a) and decreases due to the conversion mechanism. In addition, it broadens slightly with increasing z which can be understood as follows. For the given parameters the Rayleigh length $z_M = \pi\sigma_M^2/\lambda_M$ of the mm-wave is $z_M \approx 11.3\lambda_M$, which is about half the length of the medium. The broadening is thus caused by the strong focussing of the beam before it enters the atomic ensemble. Note that the Rayleigh length is much larger than the wavelength λ_M, and hence the paraxial approximation is justified. The intensity of the optical wave is shown in figure 6(a) and increases with increasing z. In order to quantify the conversion efficiency, we consider the total power of the incoming mm-wave and of the outgoing optical field

$$P_M^{in} = \frac{\pi\varepsilon_0 c\hbar^2}{|\boldsymbol{d}_{34}|^2} \int_0^\infty |\Omega_M(z = 0,\ r)|^2 r\ dr, \tag{33a}$$

$$P_L^{out} = \frac{\pi\varepsilon_0 c\hbar^2}{|\boldsymbol{d}_{16}|^2} \int_0^\infty |\Omega_L(z = L_c,\ r)|^2 r\ dr, \tag{33b}$$

where ε_0 is the dielectric constant. We then define the conversion efficiency by

$$F = \frac{\omega_M}{\omega_L} \frac{P_L^{out}}{P_M^{in}}, \tag{34}$$

which is consistent with our definition of the conversion efficiency in section 3.1. We find $F \approx 26\%$ for the parameters in figure 6, and this value can be further increased by increasing the transverse size of the atomic

cloud. For example, for an atomic ensemble with transverse size $\sigma_c \approx 1$ mm we obtain $F \approx 61\%$. In addition, the conversion of optical fields to mm-waves works equally well. For a Gaussian optical beam of width $\sigma_L \approx 509$ μm and all other parameters as in figure 6, we find $F \approx 24\%$. This value increases to $F \approx 72\%$ if the atomic cloud size is increased to $\sigma_c \approx 1$mm. However, increasing the transverse size of the atomic ensemble requires auxiliary fields with higher power in order to maintain the intensities shown in figure 5.

Next we discuss the implementation shown in figure 1(b), where the mm-waves are confined by a waveguide and an elongated atomic cloud is trapped inside the waveguide core. This setting can be approximately described by the one-dimensional model in equation (10) if the ratio of the coupling constants in equation (8) is replaced by

$$b_{\rm wg}^2 = \frac{A_{\rm L}}{A_{\rm M}} b^2, \tag{35}$$

where $A_{\rm M}$ is the effective area of the mm-wave guided mode, and $A_{\rm L}$ is the transverse size of the optical beam which is assumed to match the transverse density profile of the atoms [35, 53]. In principle, the setup in figure 1(b) can thus be employed to interconvert mm-waves with longer wavelengths that cannot be focussed down to realistic dimensions of cold atom clouds. However, since $A_{\rm L}/A_{\rm M} \ll 1$, this results in smaller values of the parameter $\varepsilon \propto b_{\rm wg}$ defined in equation (24) and thus in larger values of the optical depth required for complete conversion, $D_c = \pi/(2\varepsilon)$. In order to achieve the required optical depths, the atoms could be confined inside hollow core fibres where extremely large optical depths have been observed [54, 55]. In addition, mm-waves can similarly be guided by photonic crystal fibres [56]. The strong coupling of atoms with mm-wave and optical fields required for efficient conversion might then be achievable by embedding a small hollow-core photonic crystal fibre into a larger mm-wave photonic crystal fibre.

4. Summary

We have shown that frequency mixing in Rydberg gases enables the coherent conversion between mm-wave and optical fields. Due to the numerous possibilities for choosing the $|3\rangle \leftrightarrow |4\rangle$ transition within the Rydberg manifold, our proposed MMOC scheme enables the conversion of various frequencies ranging from terahertz radiation to the microwave spectrum, that is for frequencies in the range 10–10 000 GHz. The degree of conversion can be adjusted through the atomic density and the ancillary drive field intensities and frequencies. Conversion efficiencies are limited by the lifetime of the Rydberg levels and dipole–dipole interactions between Rydberg atoms. Imperfections due to Rydberg interactions can be minimised in ensembles with low atomic densities and by the choice of the atomic states and parameters of the auxiliary fields. We have analysed a realistic implementation for the interconversion of terahertz and optical fields with an ensemble of trapped rubidium atoms, and find that the conversion efficiency can exceed 90%.

Efficient conversion requires a large spatial overlap between the mm-wave and optical fields, and we have discussed two possible scenarios how to achieve this. First, we have considered focussed terahertz beams and found that high conversion efficiencies are possible if the Rayleigh length of the beams is comparable to the length of the atomic cloud. Second, we investigated a setup where the mm-wave fields are transversally confined by a waveguide and the atoms are trapped inside the waveguide core. The optical depth required for complete conversion increases by $\sqrt{A_{\rm M}/A_{\rm L}}$ compared to the free-space implementation, where $A_{\rm M}$ is the effective area of the mm-wave guided mode and $A_{\rm L}$ is the transverse size of the atomic cloud. This waveguide setting enables high conversion efficiencies close to the theoretical limit set by the lifetime of the Rydberg states and Rydberg interactions.

Acknowledgments

We thank the National Research Foundation and the Ministry of Education of Singapore for support. The research leading to these results has received funding from the European Research Council under the European Union's Seventh Framework Programme (FP7/2007-2013)/ERC Grant Agreement no. 319286 Q-MAC, and from the UK EPSRC through the standard grant EP/J000051/1, the programme grant EP/K034480/1 and through the Hub for Networked Quantum Information Technologies (NQIT). JN acknowledges support from a Royal Society University Research Fellowship.

Appendix. Atomic coherences

Here we derive the adiabatic solutions for the atomic coherences ϱ_{43} and ϱ_{61} in equation (9). To this end, we assume that the fields $\Omega_{\rm M}$ and $\Omega_{\rm L}$ are sufficiently weak and expand the atomic density operator as follows

[57, 58]

$$\varrho = \sum_{k=0}^{\infty} \varrho^{(k)}, \tag{A1}$$

where $\varrho^{(k)}$ denotes the contribution to ϱ in kth order in the Hamiltonian

$$H_{\rm I} = -\hbar\,(\Omega_{\rm M} A_{43} + \Omega_{\rm L} A_{61}) + {\rm h.c.}. \tag{A2}$$

The solutions $\varrho^{(k)}$ can be obtained by re-writing the master equation (1) as

$$\mathcal{L}\varrho = \mathcal{L}_0 \varrho - \frac{\rm i}{\hbar}[H_{\rm I},\, \varrho], \tag{A3}$$

where the linear super-operator $\mathcal{L}_0$ is independent of $\Omega_{\rm M}$ and $\Omega_{\rm L}$. Inserting the expansion (A1) into equation (A3) leads to the following set of coupled differential equations

$$\dot{\varrho}^{(0)} = \mathcal{L}_0 \varrho^{(0)}, \tag{A4}$$

$$\dot{\varrho}^{(k)} = \mathcal{L}_0 \varrho^{(k)} - \frac{\rm i}{\hbar}[H_{\rm I},\, \varrho^{(k-1)}], \quad k > 0. \tag{A5}$$

Equation (A4) describes the interaction of the atom with the fields $\Omega_{\rm P}$, $\Omega_{\rm R}$, $\Omega_{\rm C}$ and $\Omega_{\rm A}$ to all orders and in the absence of $H_{\rm I}$. Higher-order contributions to ϱ can be obtained if equation (A5) is solved iteratively. Equations (A4) and (A5) must be solved under the constraints ${\rm Tr}(\varrho^{(0)}) = 1$ and ${\rm Tr}(\varrho^{(k)}) = 0$ $(k > 0)$.

The zeroth-order solution $\varrho^{(0)}$ is the EIT dark state of the three-level ladder system $|1\rangle$, $|2\rangle$ and $|3\rangle$. For the special case $\Delta_3 = 0$ and if the small decay rate Γ of state $|3\rangle$ is neglected, we find

$$\varrho_{11}^{(0)} = \frac{|\Omega_{\rm R}|^2}{|\Omega_{\rm P}|^2 + |\Omega_{\rm R}|^2}, \tag{A6a}$$

$$\varrho_{33}^{(0)} = \frac{|\Omega_{\rm P}|^2}{|\Omega_{\rm P}|^2 + |\Omega_{\rm R}|^2}, \tag{A6b}$$

$$\varrho_{13}^{(0)} = -\frac{\Omega_{\rm P}^* \Omega_{\rm R}^*}{|\Omega_{\rm P}|^2 + |\Omega_{\rm R}|^2}. \tag{A6c}$$

For $|\Omega_{\rm P}| \ll |\Omega_{\rm R}|$ the steady state is reached within several inverse decay times $1/\gamma$.

In general, we obtain the zeroth-order solution $\varrho^{(0)}$ for $\Delta_3 \neq 0$ and substitute it in the first-order equation (A5) with $k = 1$. The formal solution of this differential equation is given by

$$\begin{aligned}\varrho^{(1)}(t) = &\frac{\rm i}{\hbar}\mathcal{L}_0^{-1}[H_{\rm I}(t),\, \varrho^{(0)}] \\ &- \frac{\rm i}{\hbar}\mathcal{L}_0^{-1}\int_0^t {\rm d}t' {\rm e}^{\mathcal{L}_0(t-t')}\partial_{t'}([H_{\rm I}(t'),\, \varrho^{(0)}]),\end{aligned} \tag{A7}$$

where we assumed $H_{\rm I}(0) = 0$. If $H_{\rm I}(t)$ varies sufficiently slowly with time, the second term on the right-hand side in equation (A7) involving the time derivative of $H_{\rm I}$ can be neglected. More precisely, this approximation is justified if the bandwidth δ_ν of the pulses $\Omega_{\rm M}$ and $\Omega_{\rm L}$ is small as compared to the relevant differences between eigenfrequencies of H_0. Through a numerical study we find that this condition is satisfied if all detunings Δ_k $(k \in \{4,\, 5,\, 6\})$ and the Rabi frequencies $\Omega_{\rm R}$, $\Omega_{\rm C}$ and $\Omega_{\rm A}$ are large as compared to the bandwidth δ_ν. In general, the analytical expression for the first-order density operator ϱ is too bulky to display here. A special solution if the conditions in equation (22) are met is given in equation (23*a*).

References

[1] Fortier T *et al* 2011 *Nat. Photon.* **5** 425
[2] Martin R *et al* 2012 *SPIE Newsroom* (doi:10.1117/2.1201208.004406)
[3] Yang X, Xu K, Yin J, Dai Y, Yin F, Li J, Lu H, Liu T and Ji Y 2014 *Opt. Express* **22** 869
[4] Loïc M *et al Int. Radar Conf.—Surveillance for a Safer World, 2009, RADAR* (Piscataway, NJ: IEEE) pp 1–5
[5] Adam A J L 2011 *J. Infrared Milli. Terahz. Waves* **32** 976
[6] Chan W L, Deibel J and Mittleman D M 2007 *Rep. Prog. Phys.* **70** 1325
[7] Barrett S D and Kok P 2005 *Phys. Rev.* A **71** 060310
[8] Monroe C, Raussendorf R, Ruthven A, Brown K, Maunz P, Duan L-M and Kim J 2014 *Phys. Rev.* A **89** 022317
[9] Nemoto K, Trupke M, Devitt S J, Stephens A M, Scharfenberger B, Buczak K, Nöbauer T, Everitt M S, Schmiedmayer J and Munro W J 2014 *Phys. Rev.* X **4** 031022
[10] Morton J J and Mølmer K 2015 *Nature* **517** 153
[11] Barendst R *et al* 2014 *Nature* **508** 500
[12] Wallraff A, Schuster D I, Blais A, Frunzio L, Huang R-S, Majer J, Kumar S, Girvin S M and Schoelkopf R J 2004 *Nature* **431** 162
[13] Andrews R, Peterson R, Purdy T, Cicak K, Simmonds R, Regal C and Lehnert K 2014 *Nat. Phys.* **10** 321
[14] Bagci T *et al* 2014 *Nature* **507** 81
[15] Xia K, Vanner M R and Twamley J 2014 *Sci. Rep.* **4** 5571

[16] Williamson L A, Chen Y-H and Longdell J J 2014 *Phys. Rev. Lett.* **113** 203601
[17] O'Brien C, Lauk N, Blum S, Morigi G and Fleischhauer M 2014 *Phys. Rev. Lett.* **113** 063603
[18] Blum S, O'Brien C, Lauk N, Bushev P, Fleischhauer M and Morigi G 2015 *Phys. Rev.* A **91** 033834
[19] Hafezi M, Kim Z, Rolston S, Orozco L, Lev B and Taylor J 2012 *Phys. Rev.* A **85** 020302
[20] Marcos D, Wubs M, Taylor J, Aguado R, Lukin M and Sørensen A S 2010 *Phys. Rev. Lett.* **105** 210501
[21] Huber B, Kölle A and Pfau T 2014 *Phys. Rev.* A **90** 053806
[22] Che J, Ma J, Zheng H, Zhang Z, Yao X, Zhang Y and Zhang Y 2015 *Europhys. Lett.* **109** 33001
[23] Zhang Z, Che J, Zhang D, Liu Z, Wang X and Zhang Y 2015 *Opt. Express* **23** 13814
[24] Sedlacek J A, Schwettmann A, Kübler H, Löw R, Pfau T and Shaffer J P 2012 *Nat. Phys.* **8** 819
[25] Gordon J A, Holloway C L, Schwarzkopf A, Anderson D A, Miller S, Thaicharoen N and Raithel G 2014 *Appl. Phys. Lett.* **105** 024104
[26] Fan H, Kumar S, Sedlacek J, Kübler H, Karimkashi S and Shaffer J P 2015 *J. Phys.* B **48** 202001
[27] Petrosyan D, Bensky G, Kurizki G, Mazets I, Majer J and Schmiedmayer J 2009 *Phys. Rev.* A **79** 040304(R)
[28] Pritchard J D, Isaacs J A, Beck M A, McDermott R and Saffman M 2014 *Phys. Rev.* A **89** 010301(R)
[29] Fleischhauer M, Imamoğlu A and Marangos J P 2005 *Rev. Mod. Phys.* **77** 633
[30] Zhang Y, Khadka U, Anderson B and Xiao M 2009 *Phys. Rev. Lett.* **102** 013601
[31] Zhang S, Robicheaux F and Saffman M 2011 *Phys. Rev.* A **84** 043408
[32] Arimondo E 1996 *Progress in Optics* ed E Wolf vol 35 (Amsterdam: Elsevier) pp 258
[33] Cohen-Tannoudji C, Diu B and Laloë F 1977 *Quantum Mechanics* vol I (London: Wiley)
[34] Fleischhauer M and Lukin M D 2002 *Phys. Rev.* A **65** 022314
[35] Hafezi M, Chang D E, Gritsev V, Demler E and Lukin M 2012 *Phys. Rev.* B **85** 013822
[36] Zimmer F E, Otterbach J, Unanyan R G, Shore B W and Fleischhauer M 2008 *Phys. Rev.* A **77** 063823
[37] Singer K, Stanojevic J, Weidemüller M and Cote R 2005 *J. Phys.* B **38** S295
[38] Peyronel T, Firstenberg O, Liang Q-Y, Hofferberth S, Gorshkov A V, Pohl T, Lukin M D and Vuletić V 2012 *Nature* **488** 57
[39] Gallagher T F 1994 *Rydberg Atoms* (Cambridge: Cambridge University Press)
[40] Chandrasekhar S 1943 *Rev. Mod. Phys.* **15** 1
[41] Wang T, Yelin S F, Cote R, Eyler E E, Farooqi S M, Gould P L, Kostrun M, Tong D and Vrinceanu D 2007 *Phys. Rev.* A **75** 033802
[42] Bendkowsky V, Butscher B, Shaffer J N J P, Löw R and Pfau T 2009 *Nature* **458** 1005
[43] Weatherill K J, Pritchard J D, Abel R P, Bason M G, Mohapatra A K and Adams C S 2008 *J. Phys.* B **41** 201002
[44] Han J, Vogt T, Manjappa M, Guo R, Kiffner M and Li W 2015 *Phys. Rev.* A **92** 063824
[45] Pritchard J D, Weatherill K J and Adams C S 2013 *Annual Review of Cold Atoms and Molecules* ed K Madison *et al* vol 1 (Singapore: World Scientific) pp 301
[46] Beterov I I, Ryabtsev I I, Tretyakov D B and Entin V M 2009 *Phys. Rev.* A **79** 052504
[47] Steck D A Rubidium 87 D Line Data (http://steck.us/alkalidata)
[48] Walker T G and Saffman M 2008 *Phys. Rev.* A **77** 032723
[49] Petrosyan D, Höning M and Fleischhauer M 2013 *Phys. Rev.* A **87** 053414
[50] Gärttner M, Whitlock S, Schönleber D W and Evers J 2014 *Phys. Rev.* A **89** 063407
[51] Hsiao Y-F, Chen H-S, Tsai P-J and Chen Y-C 2014 *Phys. Rev.* A **90** 055401
[52] Sparkes B, Bernu J, Hosseini M, Geng J, Glorieux Q, Altin P, Lam P, Robins N and Buchler B 2013 *J. Phys.: Conf. Ser.* **467** 012009
[53] Kiffner M and Hartmann M J 2010 *Phys. Rev.* A **82** 033813
[54] Vorrath S, Möller S A, Windpassinger P, Bongs K and Sengstock K 2010 *New. J. Phys.* **12** 123015
[55] Blatt F, Halfmann T and Peters T 2014 *Opt. Lett.* **39** 446
[56] Han H, Park H, Cho M and Kim J 2002 *Appl. Phys. Lett.* **80** 2634
[57] Kiffner M and Marzlin K-P 2005 *Phys. Rev.* A **71** 033811
[58] Kiffner M, Dorner U and Jaksch D 2012 *Phys. Rev.* A **85** 023812